Journal of Power Sources 247 (2014) 452–459

Contents lists available at ScienceDirect

Journal of Power Sources

journal homepage: www.elsevier.com/locate/jpowsour

Controlled Li^+ conduction pathway to achieve enhanced ionic conductivity in polymer electrolytes

Yu Wang, Bin Li, Jianying Ji, Wei-Hong Zhong*

School of Mechanical and Materials Engineering, Washington State University, Pullman, WA 99164, USA

HIGHLIGHTS

- Core–shell structure can be used to control the ion conductive pathway.
- 3D network of ion conductive pathway in the amorphous phase improves the ion conductivity.
- Ratio plot is proposed to analyze the impedance spectrum.

GRAPHICAL ABSTRACT

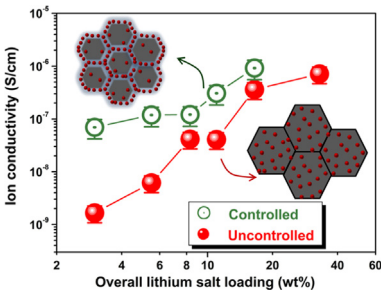

ARTICLE INFO

Article history:
Received 8 July 2013
Received in revised form
25 August 2013
Accepted 28 August 2013
Available online 11 September 2013

Keywords:
Polymer electrolytes
Conduction pathway
Ion distribution
Core–shell structure
Morphology

ABSTRACT

Low ionic conductivity is one of the issues for polymer electrolytes to be used in commercial batteries, though they have been viewed as the promising electrolytes in all-solid lithium-ion batteries for several decades. Here, we show an enhanced ionic conductivity in a classic polymer electrolyte by controlling the ionic conductive pathway via a core–shell structure. The enhancement in ionic conductivity is contributed from the formation of a controlled 3D network of the ion conductive amorphous phase. The result suggests that the core–shell structure design can realize the control of the conduction pathway, which is significant for understanding the ionic conductive behaviors as well as for the improvement of the ionic conductivity in polymer electrolytes.

1. Introduction

Solid polymer electrolytes have attracted intense attention for several decades because of the superiority in safety and also mechanical properties as compared with liquid electrolytes [1–7]. However, it is well-known that the biggest challenge for solid polymer electrolytes is their very low ionic conductivity, which limits their viability for commercial application [8–10]. To overcome this challenge, the understanding of the ionic conductive behavior as well as effective approach to the improvement of the ionic conductivity is critical.

Thus far, the knowledge on the mechanisms of the ion transportation is mainly from the molecular dynamics (MD) simulations [11–16]. Via the MD simulation on amorphous poly(ethylene oxide) (PEO) electrolyte, it has been concluded that the lithium transport actually arises from a combination of the diffusion of the Li^+ along PEO chains, the motion together with PEO chain segments and also the "hopping" from one chain segment to another [15]. These findings indicate that the dynamics of polymer chains is critical for

* Corresponding author. Tel.: +1 509 335 7658; fax: +1 509 335 4662.
E-mail address: katie_zhong@wsu.edu (W.-H. Zhong).

0378-7753/$ – see front matter © 2013 Elsevier B.V. All rights reserved.
http://dx.doi.org/10.1016/j.jpowsour.2013.08.137

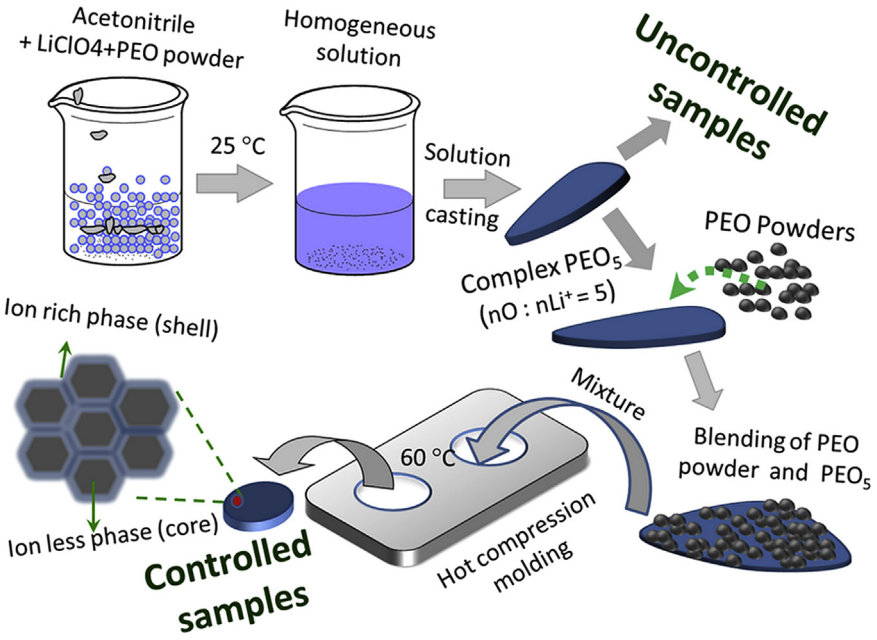

Fig. 1. Procedures for the preparation of electrolyte samples with uncontrolled and controlled ions conduction pathway.

the ion transportation. Therefore, many efforts [12,13] can be found on how the ions are coupled with the chain dynamics by the help of some classical dynamics models for polymer chains, for example, Rouse model [17]. This couple effect between the ions and the polymer chains seem to be the main reason for the low ionic conductivity of polymer electrolytes as proven by experimental results. For example, the ionic conductivity was found to decrease with the increasing of the molecular weight of polymers [18], or increase with the addition of various plasticizers [19–22]. However, this popular view has been questioned by Agapov [23], Fullerton-Shirey et al. [24,25] based on some new results showing a decoupling of the ionic conductivity and polymer mobility. This inconsistency indicates that the interaction between the ions and polymer host is very complicated.

At the same time, polymer electrolytes usually feature multiphase structures in macroscopic levels, which can make the ion transport very complex. Firstly, the coexistence of different phases, such as amorphous phase and various crystalline complexes of PEO and Li^+ [24,26], provides different pathways for the ion transportation; secondly, the distribution and structure of the phases are also intricate. In particular, the understanding of the ion transport in amorphous and crystalline phases is still controversial: the prevailing view is that the ions move faster in the amorphous phase than it does in the crystalline phase; however, the work by Bruce et al. [27,28] supports the opposite result. It is difficult to settle this dispute since we are unable to prepare two electrolyte samples using the same polymer: one with fully amorphous structure and the other with fully crystalline complex structure.

In spite of these difficulties, the work on the control of the morphology structures to improve the ion conductivity is meaningful not only for the understanding of how morphology structures contribute to the ion conductivity, but also guiding the structure design to improve the ion conductivity. For example, by composites [1,29–32], stretching [33,34] or electromagnetic fields [35,36], an improvement of ion conductivity can be achieved. In particular, anisotropic ion conductive behaviors [37–40] can be observed in copolymer electrolytes. These findings indicate that a controlled morphology or ion conductive pathway is very significant for polymer electrolytes.

Here, without addition of any nanoparticles or plasticizers, we show that the ionic conductivity indeed can be improved by only a controlled Li^+ conduction pathway. The method we applied to realize the control of the ion pathway is based on a core–shell structure.

2. Experimental

2.1. Materials

The polymer used to prepare the polymer electrolyte samples is poly(ethylene oxide) (PEO, $M_w = 10^5$ g mol^{-1}, Sigma Aldrich). The lithium salt is lithium perchlorate ($LiClO_4$, Sigma Aldrich). The solvent employed to distribute the lithium salt is acetonitrile (A.C.S. Reagent). The polymer PEO and the lithium salt were dried at 70 °C for at least 12 h before using.

2.2. Electrolyte preparation

As shown in Fig. 1, the *uncontrolled* samples were prepared by the common solution casting. This method gives rise to a relatively homogeneous distribution of ions. Specifically, the lithium salt was dissolved first in the solvent acetonitrile, and then PEO powder was added into the solution and was dissolved under stirring condition for 24 h. Finally, the homogeneous solution was solution casted at room temperature. Several compositions, as listed in Table 1, were used to prepare the uncontrolled samples.

Table 1
Information of the electrolyte samples used in this work.

Controlled		Uncontrolled
PEO_5 content (wt%)	Lithium salt content (wt%)	Lithium salt content (wt%)
50	17	17
33	11	11
25	8	8
17	6	6
9	3	3

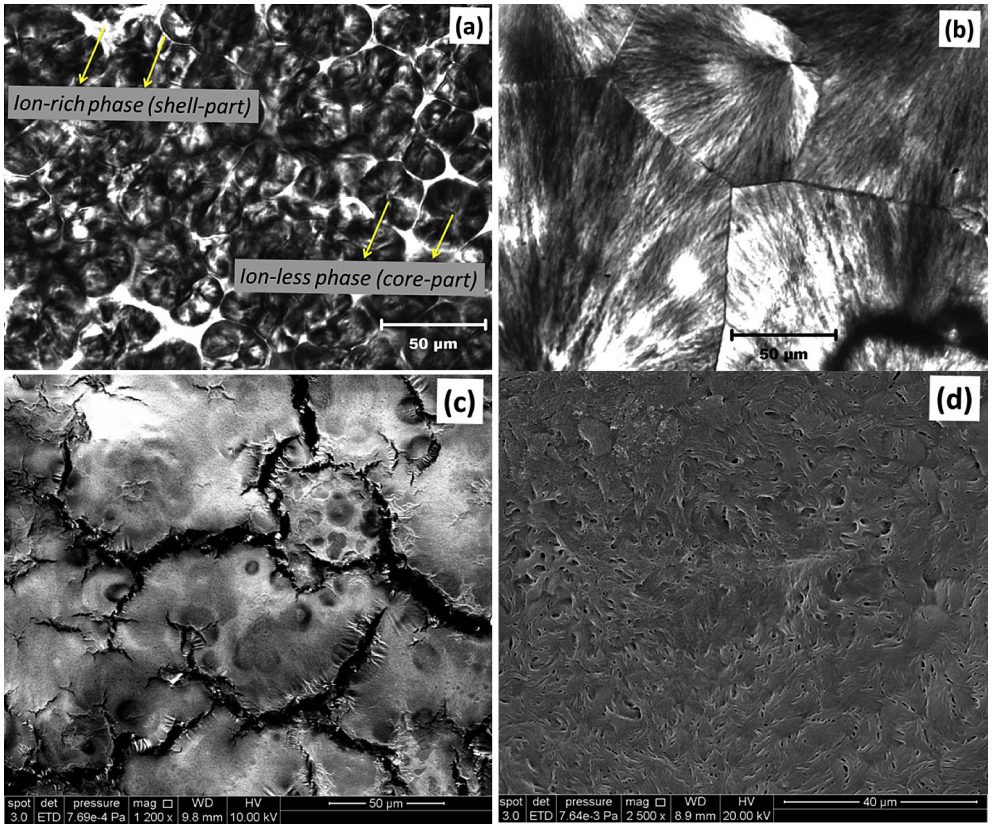

Fig. 2. Polar light microscopic images (a) and (b) and SEM images (c) and (d) for the controlled and uncontrolled electrolyte samples respectively.

To prepare the *controlled* sample, the uncontrolled sample with the highest content of lithium salt (nO:nLi$^+$ = 5, referred to as the complex PEO_5) was first prepared. In order to control the ion conductive pathway, PEO_5 was purposely blended with the PEO powders at room temperature. The PEO powders are used as received and the average size of the particles is ca. 33 μm. At the same time, to coat the PEO powders with the complex PEO_5 as uniformly as possible, the PEO powders were scattered on a thin layer of complex PEO_5, and they were mixed at room temperature. To remove the air bubbles introduced during the mixing, the mixture was further compressed (5 MPa at 60 °C) in a metal mold for 5 min. The temperature used for the hot compression is lower than the melting point of PEO (ca. 70 °C), in order to avoid the melting of PEO and suppress the diffusion of lithium ions into the core part (i.e. the PEO powders), during the hot compression. For the same purpose, a low pressure of 5 MPa was used. By varying the weight ratio of PEO_5 to the PEO powders, the thickness of the shell part can be controlled as PEO_5 will constitute the shell part in the core–shell structure. The weight fraction of the complex PEO_5 used in this work as well as the sample compositions are shown in Table 1.

2.3. AC conductivity and structural characterization of electrolytes

The AC conductivity (the real part of the complex conductivity, $\sigma^*(\omega) = \sigma'(\omega) + i\sigma''(\omega)$) was obtained by AC impedance spectroscopy measurements (Universal Dielectric Spectrometer BDS 20). The specific testing conditions are as following. The frequency range was chosen to be 10^{-1} Hz–10^6 Hz and, the electrolyte sample was sandwiched between two gold electrodes of 2 cm diameter. The input voltage for the measurement was 1 V. To investigate the aging properties of the polymer electrolytes, the AC conductivity of one electrolyte sample from the controlled group with 11 wt% of lithium salt was measured after different storage times at room temperature. At the same time, for comparison, another electrolyte sample from the uncontrolled group was also measured under the same conditions.

The microstructures of the electrolyte samples were analyzed using a polarized light microscope (Olympus BX51) at room temperature. To prove the core–shell structure in the controlled electrolyte samples, Differential Scanning Calorimetry (DSC) was used. The heating curve with a speed of 10 °C min^{-1} and in the range from 20 °C to 150 °C was recorded for analysis. Scanning Electron Microscopy (SEM) was also used to observe the phase morphology of the electrolytes.

3. Results and discussion

3.1. Morphology structures

The typical morphological structures for the controlled and uncontrolled samples are shown in Fig. 2. For the controlled sample, two very different phases are clearly seen from a core–shell configuration as indicated in Fig. 2(a). It is noted that the complex PEO_5 was found to be almost amorphous [41] because of the high content of lithium salt, which will be confirmed by its melting behavior later. Therefore, the bright stream-like part constitutes the "ion-rich" phase, that is, the complex PEO_5; the dark part is the pure PEO powder, the "ion-less" phase as also indicated in Fig. 1. In addition, the average size of the core-part (ca. 45 μm) is close to that of the pristine PEO powders (ca. 33 μm). This fact further confirms that the core-part consists of the pure PEO powders. In contrast, the morphology in the uncontrolled samples is uniform as shown in Fig. 2(b). At the same time, SEM images of the controlled samples

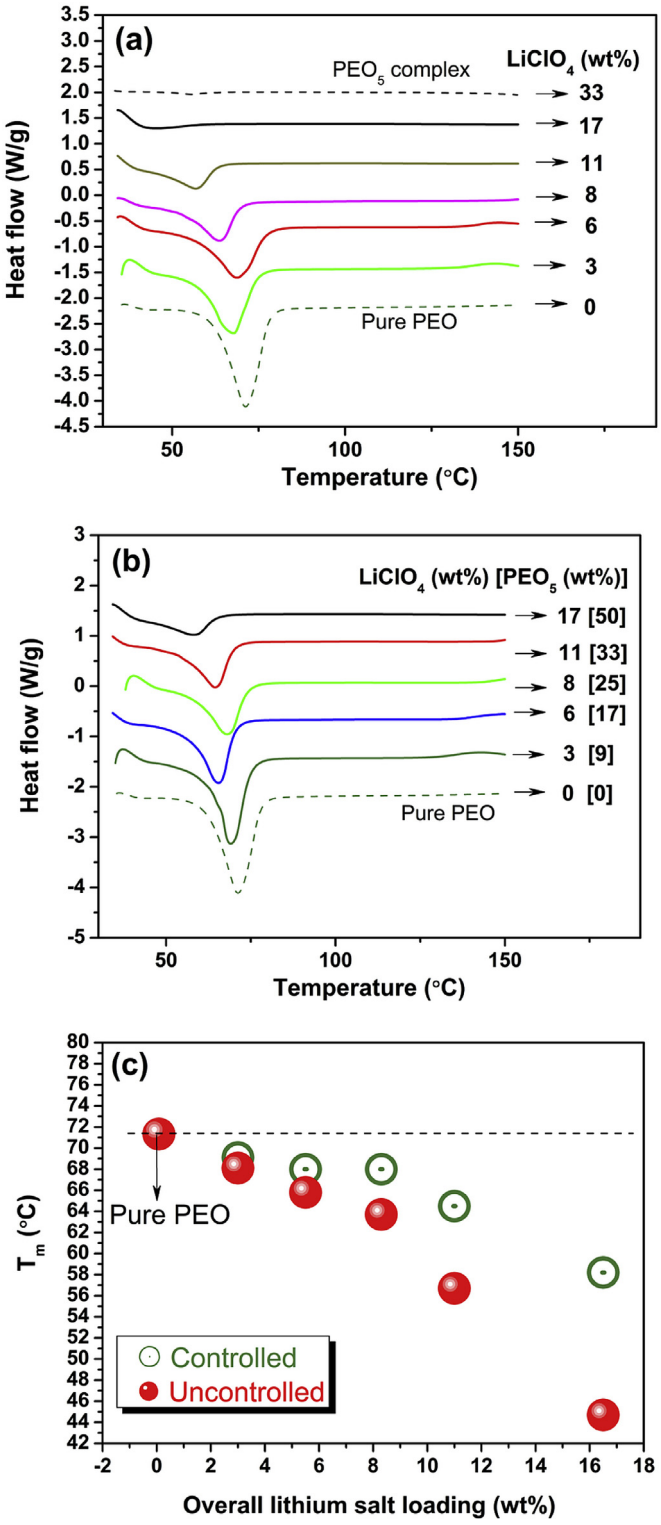

Fig. 3. Melting behaviors of the uncontrolled (a) and controlled (b) polymer electrolyte samples (vertical translation is used to separate the curves); (c) comparison of the melting point for the pure PEO in the controlled and uncontrolled samples.

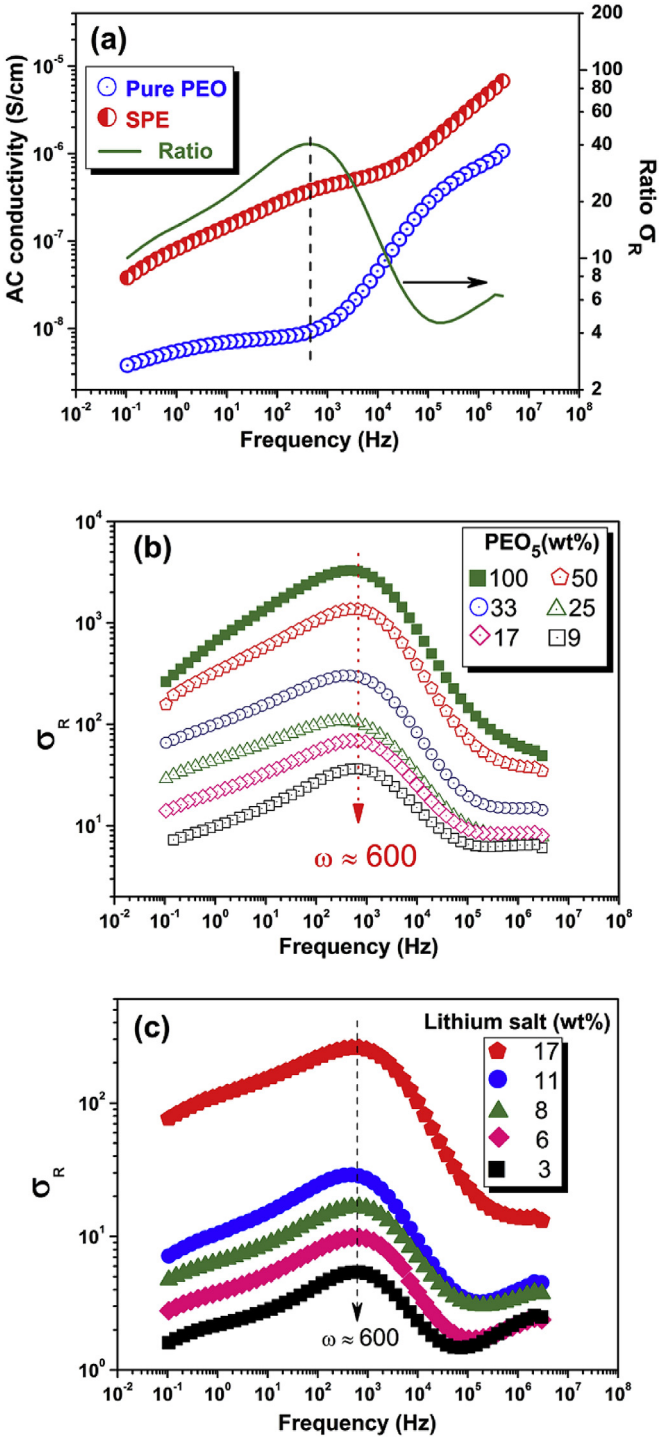

Fig. 4. The definition of the ratio plot for conductivity (a) and the ratio plots for the controlled (b) and uncontrolled (c) SPEs.

can reveal the inhomogeneous morphology related to the core–shell structure. As shown in Fig. 2(c), many cracks can be found on the fractured surface. These cracks are likely caused by non-uniform contractions during the treatment in liquid nitrogen, resulting from inhomogeneous morphological structures: the core–shell structures shown in Fig. 1. SEM images also reveal a uniform morphology structure for the uncontrolled sample as displayed in Fig. 2(d).

The morphology structures for the polymer electrolytes can also be revealed by their crystallization behaviors. Due to the interaction between the lithium ions and polymer chains, the crystallization of PEO will be influenced by not only the content, but also the distribution of the lithium ions. For a fixed loading of the lithium salt, the more homogeneous the distribution of the lithium salt is, the

stronger the effects of the lithium salt on the PEO crystallization. As shown in Fig. 3(a) and (b), there is a clear melting peak related to the pure PEO component. For the PEO_5 complex, the fact that no melting peak can be found confirms that PEO_5 is amorphous. It is noted that the melting points (the temperature at the melting peak) of the pure PEO component for the controlled sample are always higher than those of the uncontrolled sample as shown in Fig. 3(c). This result should be related to a much weaker effect of lithium ions on the crystallization of PEO in the controlled samples as compared with the uncontrolled samples, which supports the core–shell configuration as shown in Fig. 1. Nevertheless, it is noted that the melting point of the core-part in the controlled samples is still lower than that of the pure PEO. This phenomenon indicates that there is ion diffusion from the shell-part into the core-part.

3.2. Ratio plot

3.2.1. Theoretical discussion

A new method, as demonstrated in Fig. 4(a) and referred to as the ratio plot below, has been employed to analyze the impedance spectrum. The ratio is defined as: $\sigma_R(\omega) = \sigma'_{SPE}(\omega)/\sigma'_{Pure\ PEO}(\omega)$, where the subscript "*SPE*" refers to the solid polymer electrolyte in this work, $\sigma'_{SPE}(\omega)$ and $\sigma'_{Pure\ PEO}(\omega)$ are the AC conductivity for the SPE and the pure PEO respectively, and ω is the frequency. There are two main advantages to use the ratio plot. Firstly, we can derive information on how the content of ions and the conducting pathway, i.e. the distribution of lithium salt, affect the ionic conductivity. Secondly, we could not only obtain the change in the magnitude of the ionic conductivity, but also the change in the ω-dependent behavior of ionic conductivity as demonstrated in Fig. 4(a). The latter is important because the ω-dependent behavior is related to the dynamics of the dipoles and ion pairs in the electrolyte.

For instance, assuming that the slope for the ω-dependent behavior of the AC conductivity in the log–log coordinate is $S(\omega)$, we will have the differential forms:

$$d\left[\lg\left(\sigma'_{SPE}(\omega)\right)\right] = S_{SPE}(\omega)d\omega \text{ for the electrolyte samples} \quad (1a)$$

$$d\left[\lg\left(\sigma'_{Pure\ PEO}(\omega)\right)\right] = S_{Pure\ PEO}(\omega)d\omega \text{ for the pure PEO} \quad (1b)$$

Further, we can find that

$$d\left[\lg\sigma'_{SPE} - \lg\sigma'_{Pure\ PEO}\right] = [S_{SPE}(\omega) - S_{Pure\ PEO}(\omega)]d\omega \quad (2a)$$

According to the definition of the ratio, we finally have

$$d(\lg\sigma_R) = [S_{SPE}(\omega) - S_{Pure\ PEO}(\omega)]d\omega = \Delta S(\omega) \quad (2b)$$

Specifically, if the slope $S_{SPE}(\omega)$ for the electrolyte sample is less than the slope $S_{Pure\ PEO}(\omega)$ for the pure PEO, then the ratio slope, $\Delta S(\omega)$, will be negative. Since a negative slope indicates that the ratio will decrease with the increasing frequency, we can conclude that the contribution from the lithium salt, assessed by the value of the ratio, to the ionic conductivity becomes weaker and weaker as the frequency increases.

3.2.2. Analysis of the electrolytes

As shown in Fig. 4(b) and (c), there are several interesting behaviors of the ratio plot which are worthy of discussion. Firstly, there is an obvious peak for the ratio plot. Secondly, the value of the ratio at the peak increases with the increasing content of the lithium salt, but the position for the peak seems to be independent of the ion distribution as well as the content of the complex or the lithium salt. Since these behaviors are definitely caused by the addition of the lithium salt, they should be related to the ion distribution, the ion content and also the interaction between the ions and the polymers as discussed below.

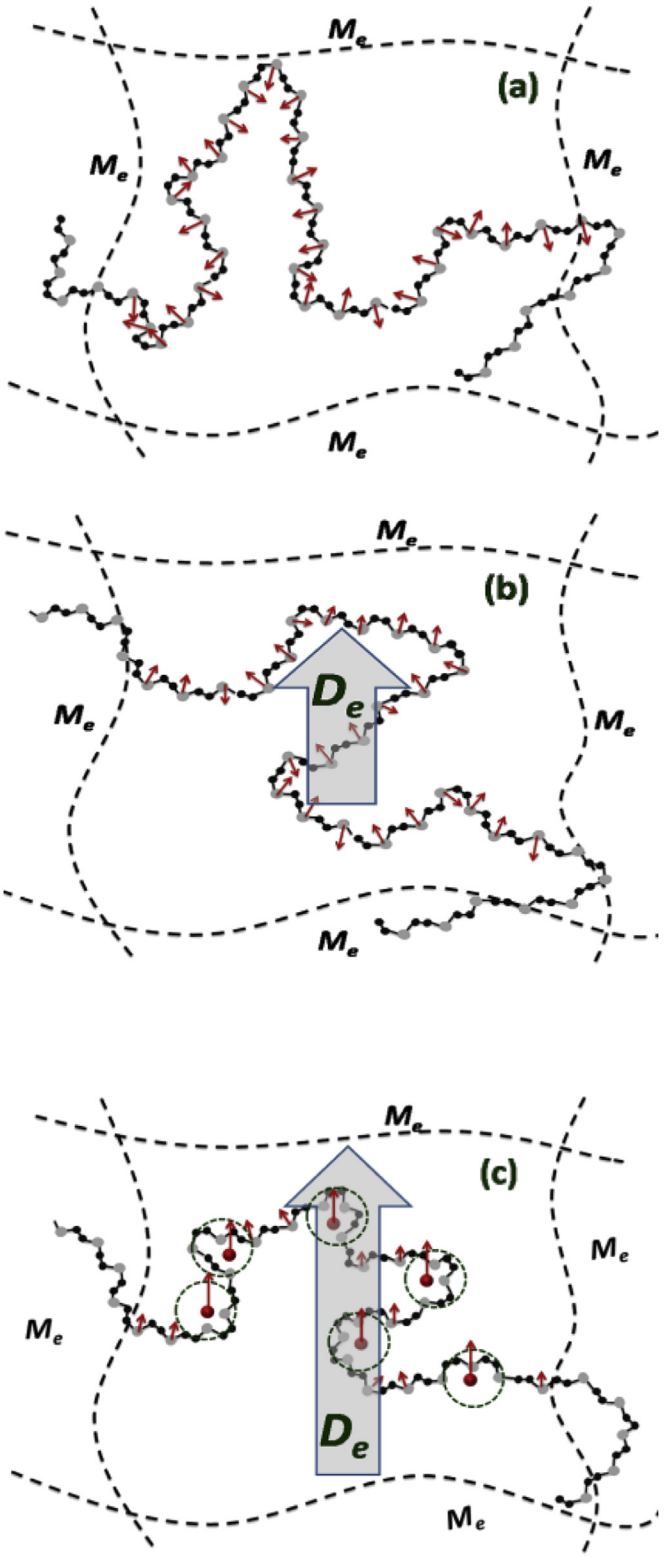

Fig. 5. Dipole orientation based on entangled segment (the dashed lines stand for the entanglement network). (a) No dipole orientation, (b) dipole orientation under electrical field and (c) enhanced dipole orientation with the addition of lithium salt (for details, see the text).

For the first point, at the peak, the ratio slope, $\Delta S(\omega)$, is equal to 0 from a mathematical point of view. This means the electrolyte

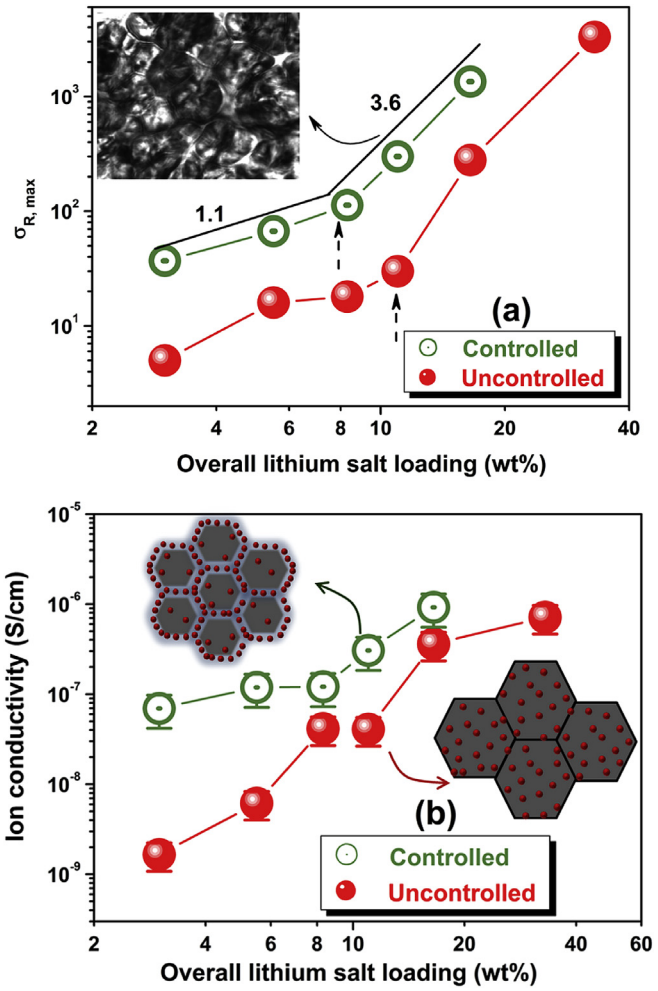

Fig. 6. Ion conductive properties for the controlled and uncontrolled SPEs: (a), peak value of the ratio and (b) ion conductivity obtained by impedance analysis.

sample shows a ω-dependent behavior as the same as the pure PEO does at the frequency of the peak. Based on the fact that the ω-dependent behaviors for the electrical properties of polymer electrolyte are determined by the dynamics of the dipoles and ions [42–44], the dipoles and ion dynamics detected at the peak frequency are not affected by the addition of the lithium salt. In fact, the dipole relaxation at the peak frequency corresponds to a transition for the AC conductivity curve as indicated by the dashed line in Fig. 4(a). Based on the finding by Ward et al. [45] that the chain entanglement structure is not affected by the addition of lithium salt, the structure determining the dipole relaxation at the peak frequency is likely related to the entanglement structure of the amorphous phase as explained below.

For pure PEO, there will be no dipole orientation within one PEO entangled segment if no electric field is applied (see Fig. 5(a)). When an electric field is applied, the O–C dipoles along the entangled segment, the segment between two continuous entanglement points in the same chain, will align with the direction of the electric field and give rise to an overall dipole for each entangled segment (called D_e as shown in Fig. 5) because of the interaction between the dipoles and the electrical field. This dipole orientation based on chain entanglements occurs at the peak frequency as shown in Fig. 4. For the SPEs, on the other hand, the applied electric field will interact more strongly with the PEO chains than in the case of pure PEO; the curved nature of the entangled segments will change, as lithium ions are predominantly coordinated by several ether oxygen atoms [46]. This change in the curve nature may facilitate the orientation of the O–C dipoles and results in a larger overall dipole along the entangled segment as shown in Fig. 5(c). Since the relaxation of the overall dipole within one entanglement is determined by the relaxation of the entanglement structure (described by the entanglement molecular weight M_e [17]), the peak position corresponding to the relaxation of D_e in the ratio plot will be independent of the content as well as the distribution of the lithium salt since the entanglement structure is not affected by the lithium salt [45].

Based on the above understanding of the peak behavior shown in the ratio plots, the content or the distribution of the ions will influence the ratio $\sigma_R(\omega)$ at its peak, $\sigma_{R,max}$. In particular, the addition of lithium salt can actually increase the content of the amorphous phase and enhance the contribution of the overall dipole associated with the entanglement structure. It is noted that the peak values of the controlled samples are much higher than those of the uncontrolled samples as shown in Fig. 6(a). This difference indicates that the peak values are related to the ion distribution.

3.3. Effects of a controlled ion-conductive pathway

The effect of the ion-conductive pathway on the ionic conductivity properties can be revealed by comparing $\sigma_{R,max}$ for the two groups at different lithium salt loading as shown in Fig. 6(a). With equal loadings of lithium salt, we can find that the controlled electrolyte sample always has a higher value of $\sigma_{R,max}$ than uncontrolled electrolyte sample. This finding indicates that a controlled ion conductive pathway, that is, the ion distribution, by the core–shell morphology structure can give a better performance on the ionic conductive properties than the samples with uncontrolled ion conductive pathway.

The lithium salt loading dependent behaviors of the conductive properties as shown in Fig. 6(a) implies the formation of a network of ion conductive pathway. For the controlled SPEs, there is a clear transition in the slope from 1.1 to 3.6 in logarithmic coordinates. A slope value ranging from 3 to 4 in logarithmic coordinates is usually caused by the formation of networks [47–50]. Therefore, this transition is the result of the formation of an ion-conducting network pathway, which is controlled by the core–shell structure and constructed by the shell part. This lithium salt loading dependent behavior is in fact determined by the morphology structure related to the lithium salt loading as explained below. Firstly, the lithium salt loading is controlled by the content of the PEO_5 complex, which is dominated by amorphous structure. Therefore, as the lithium salt loading increases, the content of amorphous phase increases correspondingly, or in other words, the thickness of the shell part increases with the increase of the lithium salt loading. Secondly, the lithium salt loading can affect the morphology structure by diffusion of ions from the complex into the pure PEO powder. This is unavoidable but the effect on the ion distribution is not critical.

It is noted that, for the uncontrolled group, there is also a transition in the lithium salt loading dependent behavior of $\sigma_{R,max}$, but the lithium salt loading for the transition is higher than that for the controlled group as indicated by the dashed arrows in Fig. 6(a). The mechanism for the transition behaviors of the two groups are in essence the same, that is, they are caused by the formation of a 3D network structure of ion conductive pathway. Since the addition of lithium salt will increase the fraction of the amorphous phase as indicated in Fig. 3, this 3D ionic conductive network can be constructed by the ion conductive amorphous phase. This finding actually agrees with the well-accepted view that the ion conduction occurs predominantly in the amorphous regions. Moreover, it

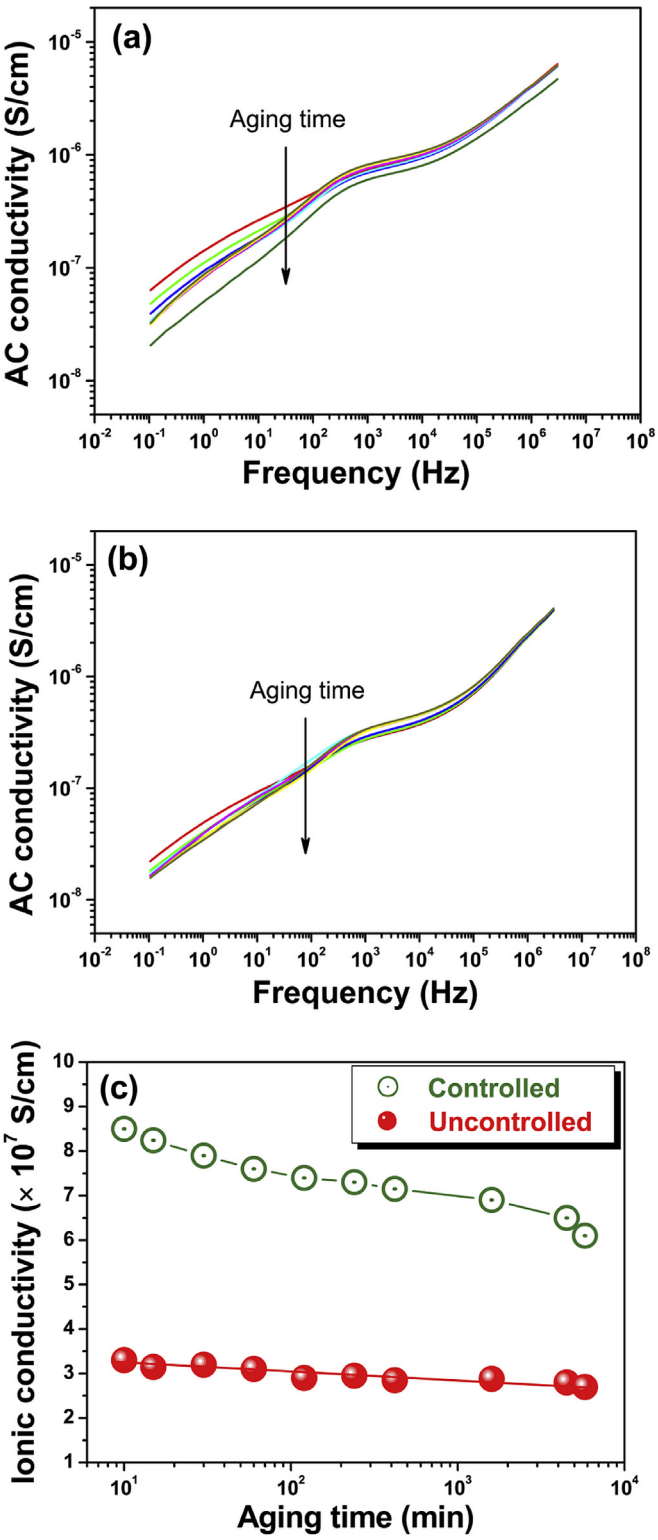

Fig. 7. Time-dependent behaviors of the AC conductivity for, (a) the controlled and, (b) the uncontrolled SPEs, (c) comparison of the time-dependent behaviors of the ionic conductivity for the two groups of SPEs.

should be pointed out that a controlled morphology structure or ion distribution is more effective to construct an ionically conductive network structure. This point can be confirmed by the fact that, as shown in Fig. 6(b), the ionic conductivity of the electrolyte sample with a controlled ion-conducting pathway, i.e., the controlled electrolyte sample, is higher than that of the electrolyte sample without any control on the ion-conducting pathway, i.e. the uncontrolled electrolyte sample. In addition, Fig. 6(b) also indicates that a controlled ion conductive pathway becomes more and more significant in improving the ion conductivity at some low loading of lithium salt.

3.4. Time-dependent behaviors

The aging property of the SPEs was investigated by tracking the conductivity property after different storage times at room temperature. As shown in Fig. 7(a) and (b), the SPEs from both the controlled and uncontrolled group show time-dependent behaviors, especially in the low frequency range. Further comparison of the aging behaviors of the ionic conductivity for the two kinds of SPEs is shown by Fig. 7(c). The ionic conductivity of the SPE from the controlled group shows a stronger time-dependent behavior than that of the SPE from the uncontrolled group. For the uncontrolled SPE, its weak time-dependent behavior is likely caused by some slow crystallization [51,52]. For the controlled SPE, the time-dependent behavior is mainly related to the change of the ion distribution since the shell-part is an ion-rich phase and the core-part is ion-poor phase as shown in Fig. 1. Although a strong time-dependent behavior reflects an unstable nature of the structures, it once again proves that a controlled distribution of ions, that is, a controlled Li^+ conductive pathway, is significant to improve the ionic conductivity property of polymer electrolyte. Designing a well-controlled core–shell structure, which is stable even at elevated temperature, may be critical for the success of polymer electrolytes with a core–shell structure.

4. Conclusions

Controlling the ion conductive path to form a 3D network structure on macroscopic scale can improve the ionic conductivity. This finding is significant for designing structures to obtain high ion conductivity in polymer electrolytes. Core–shell structure is an effective way to control the ion conductive pathway and should have the potential application to boost the ionic conductivity. Moreover, the ratio plot introduced in this study is an effective way to examine the effects of the content as well as the distribution of the lithium salt on the ionic conductivity of the polymer electrolytes.

Acknowledgment

The authors appreciate the financial support from WSU Research Advancement Challenge (RAC) Grant, “Advanced Lithium-ion Batteries Incorporating Bio-and Nano-materials and the Effects on the Agricultural Economy”.

References

[1] C.F. Yuan, J. Li, P.F. Han, Y.Q. Lai, Z.A. Zhang, J. Liu, J. Power Sources 240 (2013) 653–658.
[2] Y.S. Ye, C.Y. Tseng, W.C. Shen, J.S. Wang, K.J. Chen, M.Y. Cheng, J. Rick, Y.J. Huang, F.C. Chang, B.J. Hwang, J. Mater. Chem. 21 (2011) 10448–10453.
[3] Q.W. Lu, J.H. Fang, J. Yang, G.W. Yan, S.S. Liu, J.L. Wang, J. Membr. Sci. 425 (2013) 105–112.
[4] X. Zuo, X.M. Liu, F. Cai, H. Yang, X.D. Shen, G. Liu, J. Power Sources 239 (2013) 111–121.
[5] S.L. Zhong, C.G. Sun, Y.Q. Luo, W.C. Liu, S. Dou, J. Power Sources 238 (2013) 485–491.
[6] B. Sun, I.Y. Liao, S. Tan, T. Bowden, D. Brandell, J. Power Sources 238 (2013) 435–441.
[7] Y. Song, Y.H. Jin, Q.J. Liang, K.C. Li, Y.H. Zhang, W. Hu, Z.H. Jiang, B.J. Liu, J. Power Sources 238 (2013) 236–244.

[8] O. Buriez, Y.B. Han, J. Hou, J.B. Kerr, J. Qiao, S.E. Sloop, M.M. Tian, S.G. Wang, J. Power Sources 89 (2000) 149–155.
[9] F.B. Dias, L. Plomp, J.B.J. Veldhuis, J. Power Sources 88 (2000) 169–191.
[10] M. Park, X.C. Zhang, M.D. Chung, G.B. Less, A.M. Sastry, J. Power Sources 195 (2010) 7904–7929.
[11] V. Kuppa, E. Manias, Chem. Mat. 14 (2002) 2171–2175.
[12] A. van Zon, S.W. de Leeuw, Electrochim. Acta 46 (2001) 1539–1544.
[13] D. Diddens, A. Heuer, O. Borodin, Macromolecules 43 (2010) 2028–2036.
[14] G. Smith, O. Borodin, Abstr. Pap. Am. Chem. S. 241 (2011).
[15] O. Borodin, G.D. Smith, Macromolecules 39 (2006) 1620–1629.
[16] A. Maitra, A. Heuer, Macromol. Chem. Phys. 208 (2007) 2215–2221.
[17] J.M. Dealy, R.G. Larson, Structure and Rheology of Molten Polymers, Hanser Gardner Publications, Cincinnati, 2006.
[18] J. Shi, C.A. Vincent, Solid State Ionics 60 (1993) 11–17.
[19] Y.H. Liang, C.C. Wang, C.Y. Chen, J. Power Sources 172 (2007) 886–892.
[20] Y.J. Wang, Y. Pan, L. Wang, M.J. Pang, L.S. Chen, Mater. Lett. 59 (2005) 3021–3026.
[21] J.P. Sharma, K. Yamada, S.S. Sekhon, Ionics 18 (2012) 151–158.
[22] S. Chintapalli, R. Frech, Macromolecules 29 (1996) 3499–3506.
[23] A.L. Agapov, A.P. Sokolov, Macromolecules 44 (2011) 4410–4414.
[24] S.K. Fullerton-Shirey, J.K. Maranas, Macromolecules 42 (2009) 2142–2156.
[25] M. Marzantowicz, F. Krok, J.R. Dygas, Z. Florjanczyk, E. Zygadlo-Monikowska, Solid State Ionics 179 (2008) 1670–1678.
[26] G.S. MacGlashan, Y.G. Andreev, P.G. Bruce, Nature 398 (1999) 792–794.
[27] A.M. Christie, S.J. Lilley, E. Staunton, Y.G. Andreev, P.G. Bruce, Nature 433 (2005) 50–53.
[28] Z. Gadjourova, Y. Andreev, D. Tunstall, P. Bruce, Nature 412 (2001) 520–523.
[29] S. Bhattacharya, A. Ghosh, J. Nanosci. Nanotechnol. 8 (2008) 1922–1926.
[30] B.K. Choi, Y.W. Kim, K.H. Shin, J. Power Sources 68 (1997) 357–360.
[31] G. Derrien, J. Hassoun, S. Sacchetti, S. Panero, Solid State Ionics 180 (2009) 1267–1271.
[32] A.M. Stephan, K.S. Nahm, Polymer 47 (2006) 5952–5964.
[33] C.M. Burba, R. Frech, B. Grady, Electrochim. Acta 53 (2007) 1548–1555.
[34] C.M. Burba, L. Woods, S.Y. Millar, J. Pallie, Electrochim. Acta 57 (2011) 165–171.
[35] D. Golodnitsky, E. Livshits, R. Kovarsky, E. Peled, S.H. Chung, S. Suarez, S.G. Greenbaum, Electrochem. Solid-State Lett. 7 (2004) A412–A415.
[36] R. Kovarsky, D. Golodnitsky, E. Peled, S. Khatun, P.E. Stallworth, S. Greenbaum, A. Greenbaum, Electrochim. Acta 57 (2011) 27–35.
[37] L. Ramon-Gimenez, R. Storz, J. Haberl, H. Finkelmann, A. Hoffmann, Macromol. Rapid Commun. 33 (2012) 386–391.
[38] J. Li, K. Kamata, M. Komura, T. Yamada, H. Yoshida, T. Iyoda, Macromolecules 40 (2007) 8125–8128.
[39] P.W. Majewski, M. Gopinadhan, W.S. Jang, J.L. Lutkenhaus, C.O. Osuji, J. Am. Chem. Soc. 132 (2010) 17516–17522.
[40] P.W. Majewski, M. Gopinadhan, C.O. Osuji, J. Polym. Sci. Part B Polym. Phys. 50 (2012) 2–8.
[41] G. Mao, M.L. Saboungi, D.L. Price, Y.S. Badyal, H.E. Fischer, Europhys. Lett. 54 (2001) 347–353.
[42] R.D. Calleja, I. Devine, L. Gargallo, D. Radic, Polymer 35 (1994) 151–156.
[43] K.L. Ngai, A. Schonhals, E. Schlosser, Macromolecules 25 (1992) 4915–4919.
[44] E.E. Shafee, Eur. Polym. J. 37 (2001) 1677–1684.
[45] I.M. Ward, N. Boden, J. Cruickshank, S.A. Leng, Electrochim. Acta 40 (1995) 2071–2076.
[46] G.M. Mao, R.F. Perea, W.S. Howells, D.L. Price, M.L. Saboungi, Nature 405 (2000) 163–165.
[47] Y.Q. Tan, Y.H. Song, Q. Cao, Q.A. Zheng, Polym. Int. 60 (2011) 823–832.
[48] Q. Cao, Y.H. Song, Y.Q. Tan, Q.A. Zheng, Carbon 48 (2010) 4268–4275.
[49] X.J. Wu, Y. Wang, W. Yang, B.H. Xie, M.B. Yang, W. Dan, Soft Matter 8 (2012) 10457–10463.
[50] Y. Wang, X.-J. Wu, W. Yang, Y.-M. Zhai, B.-H. Xie, M.-B. Yang, Nanoscale Res. Lett. 6 (2011) 114–120.
[51] B.K. Choi, Y.W. Kim, Electrochim. Acta 49 (2004) 2307–2313.
[52] J.R. Dygas, B. Misztal-Faraj, Z. Floljanczyk, F. Krok, M. Marzantowicz, E. Zygadlo-Monikowska, Solid State Ionics 157 (2003) 249–256.